The Astrophysical Journal, 808:139 (14pp), 2015 August 1 doi:10.1088/0004-637X/808/2/139

EVIDENCE FOR PopIII-LIKE STELLAR POPULATIONS IN THE MOST LUMINOUS Lyα EMITTERS AT THE EPOCH OF REIONIZATION: SPECTROSCOPIC CONFIRMATION*

David Sobral[1,2,3,7], Jorryt Matthee[3], Behnam Darvish[4], Daniel Schaerer[5,6], Bahram Mobasher[4], Huub J. A. Röttgering[3], Sérgio Santos[1,2,7], and Shoubaneh Hemmati[4]
[1] Instituto de Astrofísica e Ciências do Espaço, Universidade de Lisboa, OAL, Tapada da Ajuda, PT1349-018 Lisbon, Portugal; sobral@iastro.pt
[2] Departamento de Física, Faculdade de Ciências, Universidade de Lisboa, Edifício C8, Campo Grande, PT1749-016 Lisbon, Portugal
[3] Leiden Observatory, Leiden University, P.O. Box 9513, NL-2300 RA Leiden, The Netherlands
[4] Department of Physics and Astronomy, University of California, 900 University Avenue, Riverside, CA 92521, USA
[5] Observatoire de Genève, Département d'Astronomie, Université de Genève, 51 Ch. des Maillettes, 1290 Versoix, Switzerland
[6] CNRS, IRAP, 14 Avenue E. Belin, F-31400 Toulouse, France
Received 2015 April 7; accepted 2015 June 4; published 2015 July 28

ABSTRACT

Faint Lyα emitters become increasingly rarer toward the reionization epoch ($z \sim 6$–7). However, observations from a very large ($\sim$5 deg^2) Lyα narrow-band survey at $z = 6.6$ show that this is not the case for the most luminous emitters, capable of ionizing their own local bubbles. Here we present follow-up observations of the two most luminous Lyα candidates in the COSMOS field: "MASOSA" and "CR7." We used X-SHOOTER, SINFONI, and FORS2 on the Very Large Telescope, and DEIMOS on Keck, to confirm both candidates beyond any doubt. We find redshifts of $z = 6.541$ and $z = 6.604$ for "MASOSA" and "CR7," respectively. MASOSA has a strong detection in Lyα with a line width of 386 ± 30 km s^{-1} (FWHM) and with very high EW$_0$ (>200 Å), but undetected in the continuum, implying very low stellar mass and a likely young, metal-poor stellar population. "CR7," with an observed Lyα luminosity of $10^{43.92\pm0.05}$ erg s^{-1} is the most luminous Lyα emitter ever found at $z > 6$ and is spatially extended ($\sim$16 kpc). "CR7" reveals a narrow Lyα line with 266 ± 15 km s^{-1} FWHM, being detected in the near-infrared (NIR) (rest-frame UV; $\beta = -2.3 \pm 0.1$) and in IRAC/*Spitzer*. We detect a narrow He II 1640 Å emission line (6σ, FWHM $= 130 \pm 30$ km s^{-1}) in CR7 which can explain the clear excess seen in the *J*-band photometry (EW$_0 \sim 80$ Å). We find no other emission lines from the UV to the NIR in our X-SHOOTER spectra (He II/O III] 1663 Å > 3 and He II/C III] 1908 Å > 2.5). We conclude that CR7 is best explained by a combination of a PopIII-like population, which dominates the rest-frame UV and the nebular emission, and a more normal stellar population, which presumably dominates the mass. *Hubble Space Telescope*/WFC3 observations show that the light is indeed spatially separated between a very blue component, coincident with Lyα and He II emission, and two red components ($\sim$5 kpc away), which dominate the mass. Our findings are consistent with theoretical predictions of a PopIII wave, with PopIII star formation migrating away from the original sites of star formation.

Key words: dark ages, reionization, first stars – early universe – galaxies: evolution

1. INTRODUCTION

The study of the most distant sources such as galaxies, quasars, and gamma-ray bursts offers unique constraints on early galaxy and structure formation. Such observations are particularly important to test and refine models of galaxy formation and evolution (e.g., Vogelsberger et al. 2014; Schaye et al. 2015) and to study the epoch of reionization (e.g., Shapiro et al. 1994; Furlanetto et al. 2004; Sokasian et al. 2004; Iliev et al. 2006; McQuinn et al. 2006). Over the last two decades, considerable effort has been dedicated toward finding the most distant sources. More recently, and particularly due to the upgraded capabilities of the *Hubble Space Telescope (HST)*, multiple candidate galaxies up to $z \sim 8$–11 (e.g., Bouwens et al. 2011; Ellis et al. 2013) have been found with deep broadband photometry. However, spectroscopic confirmation is still limited to a handful of galaxies and quasars at $z > 6.5$ (e.g., Mortlock et al. 2011; Ono et al. 2012; Finkelstein et al. 2013; Pentericci et al. 2014; Schenker et al. 2014; Oesch et al. 2015), for both physical (galaxies becoming increasingly fainter) and observational reasons (the need for deep near-infrared (NIR) exposures). At these redshifts ($z > 6.5$), the Lyα line is virtually the only line available to confirm sources with current instruments. However, Lyα is easily attenuated by dust and neutral hydrogen in the inter-stellar and inter-galactic medium. Indeed, spectroscopic follow-up of UV-selected galaxies indicates that Lyα is suppressed at $z > 7$ (e.g., Caruana et al. 2014; Tilvi et al. 2014) and not a single $z > 8$ Lyα emitter candidate has been confirmed yet (e.g., Sobral et al. 2009; Faisst et al. 2014; Matthee et al. 2014). If the suppression of Lyα is mostly caused by the increase of neutral hydrogen fraction toward higher redshifts, it is clear that $z \sim 6.5$ (just over 0.8 Gyr after the Big Bang) is a crucial period, because reionization should be close to complete at that redshift (e.g., Fan et al. 2006).

Narrow-band searches have been successful in detecting and confirming Lyα emitters at $z \sim 3$–7 (e.g., Cowie & Hu 1998; Malhotra & Rhoads 2004; Iye et al. 2006; Murayama et al. 2007; Hu et al. 2010; Ouchi et al. 2010). The results show that the Lyα luminosity function (LF) is constant from $z \sim 3$ to $z \sim 6$, but there are claims that the number density drops from $z \sim 6$ to $z \sim 6.6$ (e.g., Ouchi et al. 2010; Kashikawa et al. 2011) and that it drops at an even faster rate up to $z \sim 7$ (e.g., Shibuya et al. 2012; Konno et al. 2014). Moreover, the

* Based on observations obtained with X-SHOOTER, FORS2, and SINFONI on the VLT, ESO DDT time (294.A-5018, 294.A-5039) and with DEIMOS on Keck II (U082D).
[7] FCT-IF/Veni Fellow.

fact that the rest-frame UV LF declines from $z \sim 3$–6 (e.g., Bouwens et al. 2015) while the Lyα LF is roughly constant over the same redshift range (e.g., Ouchi et al. 2008) implies that the cosmic average Lyα escape fraction is likely increasing, from ~5% at $z \sim 2$ (e.g., Hayes et al. 2010; Ciardullo et al. 2014), to likely ~20%–30% around $z \sim 6$ (e.g., Cassata et al. 2015). Surprisingly, it then seems to fall sharply with increasing redshift beyond $z \sim 6.5$. Current results could be a consequence of reionization not being completed at $z \sim 6$–7, particularly when taken together with the decline in the fraction of Lyman break selected galaxies with high EW Lyα emission (e.g., Caruana et al. 2014; Pentericci et al. 2014; Tilvi et al. 2014). However, it is becoming clear that reionization by itself is not enough to explain the rapid decline of the fraction of strong Lyα emitters toward $z \sim 7$ (e.g., Dijkstra 2014; Mesinger et al. 2015).

It is likely that reionization was very heterogeneous/patchy (e.g., Pentericci et al. 2014), with the early high density regions reionizing first, followed by the rest of the Universe. If that were the case, this process could have a distinguishable effect on the evolution of the Lyα LF, and it may be that the luminous end of the LF evolves differently from the fainter end, as luminous Lyα emitters should in principle be capable of ionizing their surroundings and thus are easier to observe. This is exactly what is found by Matthee et al. (2015), in agreement with spectroscopic results from Ono et al. (2012).

In addition to using Lyα emitters to study reionization, they are also useful for identifying the most extreme, metal-poor, and young galaxies. Studies of Lyα emitters at $z > 2$–3 show that, on average, these sources are indeed very metal-poor (Finkelstein et al. 2011; Nakajima et al. 2012; Guaita et al. 2013), presenting high ionization parameters (high [O III]/Hβ line ratios; Nakajima et al. 2013) and very low typical dust extinctions (e.g., Ono et al. 2010). Given these observations, Lyα searches should also be able to find metal-free, PopIII stellar populations (since galaxies dominated by PopIII emit large amounts of Lyα photons, e.g., Schaerer 2002, 2003). However, so far, although some candidates for PopIII stellar populations have been found (e.g., Jimenez & Haiman 2006; Dijkstra & Wyithe 2007; Nagao et al. 2008; Kashikawa et al. 2012; Cassata et al. 2013), and some metal-poor galaxies have been confirmed (e.g., Prescott et al. 2009), they are all significantly more metal-rich than the expected PopIII stars, and show e.g., C III] and C IV emission. For example, when there is no evidence for the presence of an active galactic nucleus (AGN) and no metal lines, the short-lived He II 1640 Å emission line (the "smoking gun" for PopIII stars in extremely high EW Lyα emitters without any metal emission line) was never detected with high enough EW (e.g., Nagao et al. 2008; Kashikawa et al. 2012).

Until recently, Lyα studies at the epoch of reionization have been restricted to the more numerous, relatively faint sources of $L_{\mathrm{Ly}\alpha} \sim 10^{42.5}\,\mathrm{erg\,s^{-1}}$ (with some exceptions, e.g., $z = 5.7$ follow-up: Westra et al. 2006; Lidman et al. 2012; and "Himiko": Ouchi et al. 2009). However, with the wide-field capabilities of current instruments (including Hyper Suprime-Cam; Miyazaki et al. 2012), the identification of luminous Lyα emitters will become increasingly easier. Recently, significant progress was made toward finding luminous Lyα emitters at $z = 6.6$ (Matthee et al. 2015), through a ~5 deg^2 narrow-band survey, which resulted in the identification of the most luminous Lyα emitters at the epoch of reionization. Matthee et al. (2015) reproduced the Lyα LF of Ouchi et al. (2010) for relatively faint Lyα emitters at $z = 6.6$ for the UDS field, who find a decrease in their number density compared to lower redshifts. However, Matthee et al. (2015) find that the luminous end of the $z = 6.6$ LF resembles the $z = 3$–5.7 LF, and is thus consistent with no evolution at the bright end since $z \sim 3$. Extremely luminous Lyα emitters at $z \sim 6.6$ are thus found to be much more common than expected, with space densities of $1.5^{+1.2}_{-0.7} \times 10^{-5}\,\mathrm{Mpc^{-3}}$. The results may mean that, because such bright sources can be observed at $z \sim 6.6$, we are witnessing preferential reionization happening around the most luminous sources first. Such luminous sources may already be free (in their immediate surroundings) of a significant amount of neutral hydrogen, thus making their Lyα emission observable. Furthermore, these sources open a new window toward exploring the stellar populations of the most luminous Lyα emitters at the epoch of reionization even before the *James Webb Space Telescope* (*JWST*) and ~30–40 m class telescopes (Extremely Large Telescopes, ELTs) become operational, as these are bright enough to be studied in unprecedented detail with e.g., *HST*, ALMA, the Very Large Telescope (VLT), Keck.

Here we present spectroscopy of the two most luminous Lyα emitters found so far at the epoch of reionization ($z \sim 7$). This paper is organized in the following way. Section 2 presents the observations, the Lyα emitter sample, and the data reduction. Section 3 outlines the details of the optical and NIR spectroscopic observations and measurements with the VLT and Keck data. Section 4 presents the discovery of the most luminous Lyα emitters and comparison with previous studies. Section 5 discusses spectral energy distribution (SED) fitting, model assumptions and how *HST* high spatial resolution data corroborates our best interpretation of the data. Section 6 presents the discussion of the results. Finally, Section 7 outlines the conclusions. A $H_0 = 70\,\mathrm{km\,s^{-1}\,Mpc^{-1}}$, $\Omega_M = 0.3$ and $\Omega_\Lambda = 0.7$ cosmology is used. We use a Salpeter (Salpeter 1955) initial mass function (IMF) and all magnitudes are in the AB system, unless noted otherwise.

2. SAMPLE AND SPECTROSCOPIC OBSERVATIONS

2.1. The Luminous Lyα Candidates at $z = 6.6$

Matthee et al. (2015) used the Subaru telescope and the NB921 filter on Suprime-cam (Miyazaki et al. 2002) to survey ~3 deg^2 in the SA22 (PI: D. Sobral), ~1 deg^2 in COSMOS/UltraVISTA (PI: M. Ouchi) and ~1 deg^2 in UDS/SXDF (PI: M. Ouchi) fields in order to obtain the largest sample of luminous Lyα emitters at the epoch of reionization.

Out of the 135 Lyα candidates found in Matthee et al. (2015), we discover two very bright Lyα candidates in the COSMOS/UltraVISTA field: "CR7" (COSMOS Redshift 7) and MASOSA.[8] MASOSA is particularly compact (0.″7), while CR7 is extended (~3″). We show the location of the Lyα emitters within the COSMOS field footprint in Figure 1, in which the size of the symbols scales with luminosity. We also show their properties in Table 2.

[8] The nickname MASOSA consists of the initials of the first three authors of Matthee et al. (2015).

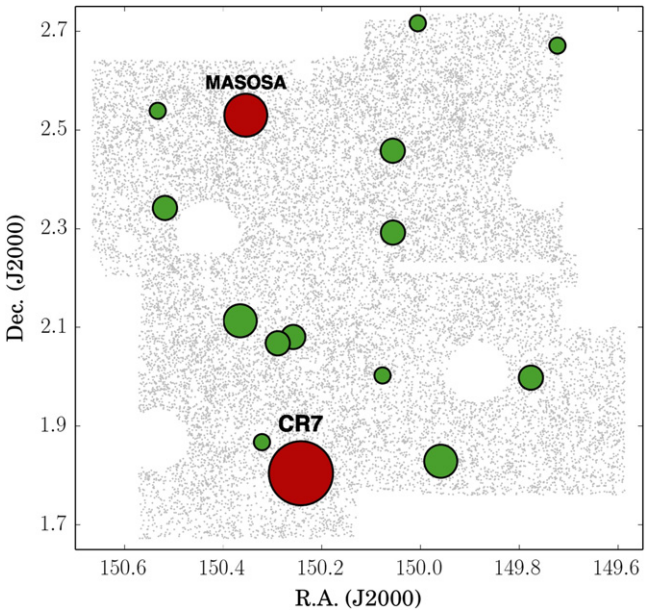

Figure 1. Projected positions on the sky of all Lyα candidates (green circles) found in the COSMOS/UltraVISTA field. The gray background points represent all detected sources with the NB921 filter, highlighting the masking applied (due to the presence of artifacts caused by bright stars and noisy regions, see Matthee et al. 2015). Lyα candidates are plotted with a symbol size proportional to their Lyα luminosity. CR7 and MASOSA are highlighted in red: these are the most luminous sources found in the field. Their coordinates are given in Table 1.

Thumbnails in various wavelengths ranging from observed optical to observed mid-infrared are shown in Figure 2. Both candidates show very high rest-frame Lyα EWs[9] in excess of >200 Å. By taking advantage of the wealth of data in the COSMOS/UltraVISTA field (e.g., Capak et al. 2007; Scoville et al. 2007; Ilbert et al. 2009; McCracken et al. 2012), we obtain multi-band photometry for both sources. The measurements are given in Table 2. We remeasure the 3.6 and 4.5 μm photometry for CR7, in order to remove contamination from a nearby source. Such contamination is at the level of 10%–20%, and is added in quadrature to the photometry errors.

We find that CR7 has very clear detections in the NIR and mid-infrared (Figure 2), showing a robust Lyman-break (Steidel et al. 1996). CR7 is detected in IRAC, with colors as expected for a $z \sim 6.6$ source (Smit et al. 2014), likely due to contribution from strong nebular lines with EWs in excess of a few 100 Å in the rest-frame optical (see Figure 2). Because of the detections in the NIR and MIR, the rest-frame UV counterpart of CR7 was already identified as a $z \sim 6$–7 Lyman-break candidate (Bowler et al. 2012, 2014). However, because of its very uncommon NIR colors (i.e., excess in J relative to Y, H, and K), the clear IRAC detections, and, particularly, without the NB921 data (Figure 2), it was classed as an unreliable candidate, possibly a potential interloper or cool star. MASOSA has a clear detection in the narrow-band and is weakly detected in z, but the z-band detection can be fully explained by Lyα. It is not detected at >1σ in the NIR ($J > 25.7$, $H > 24.5$, $K > 24.4$), although a very weak signal is visible in the thumbnails (Figure 2). This indicates that the Lyα EW is very high and highlights that the Lyman-break selection can easily miss such sources, even if they are extremely bright and compact in Lyα, as MASOSA is not detected at the current depth of the UltraVISTA survey (Bowler et al. 2014).

[9] EWs computed by using either z or Y lead to results in excess of 200 Å. We also present EWs computed based on Y band and from our spectroscopic follow-up in Table 2.

2.2. Spectroscopic Observations and Data Reduction

Spectroscopic observations were made with the VLT[10] using X-SHOOTER and SINFONI (for CR7) and FORS2 (for MASOSA). The choice of X-SHOOTER for CR7 was due to the fact that it was detected in the NIR and showed evidence for excess in the J band, likely indicating strong emission lines—SINFONI was used to confirm the results and avoid potential biases in the slit choice and inclination. Both sources were observed with DEIMOS on the Keck II telescope (see Table 1) as well. Spectra for both sources, obtained with both the VLT and Keck, are shown in Figure 3, including the spectra obtained by combining both data sets.

2.2.1. DEIMOS/Keck Observations

DEIMOS/Keck observations targeted both "CR7" and "MASOSA" in two different masks and two different nights. Observations were conducted on 2014 December 28 and 29. The seeing was ~0.″5 on the first night, when we observed "CR7," and ~0.″7 on the second night, when we observed "MASOSA." Observations were done under clear conditions with midpoint airmass of <1.1 for both sources. We used a central wavelength of 7200 Å and the 600I grating, with a resolution of 0.65 Å pix^{-1}, which allowed us to probe from 4550 to 9850 Å. We used the 0.″75 slit.

For CR7, we obtained four individual exposures of 1.2 ks and one exposure of 0.6 ks, resulting in a total of 5.4 ks. For MASOSA, we obtained a total of 2.7 ks. A strong, extended and asymmetric line is clearly seen in every individual 1.2 ks exposure prior to any data reduction.

We reduced the data using the DEIMOS SPEC2D pipeline (Cooper et al. 2012; Newman et al. 2013). The observed spectra were flat-fielded, cosmic-ray-removed, sky-subtracted, and wavelength-calibrated on a slit-by-slit basis. We used standard Kr, Xe, Ar, and Ne arc lamps for wavelength solution and calibration. No dithering pattern was used for sky subtraction. The pipeline also generates 1D spectrum extraction from the reduced 2D per slit, and we use the optimal extraction algorithm (Horne 1986). This extraction creates a one-dimensional spectrum of the target, containing the summed flux at each wavelength in an optimized window. We also extract the spectrum of both sources with varying apertures and at various positions, in order to take advantage of the fact that the sources are clearly spatially resolved. The final spectrum is shown in Figure 3.

2.2.2. FORS2/VLT Observations

FORS2/VLT (Appenzeller et al. 1998) observations targeted "MASOSA" and were obtained on 2015 January 12 and February 11. The seeing was 0.″7 and observations were done under clear conditions. We obtained individual exposures of 1 ks and applied three different offsets along the slit. In total, we obtained 6 ks. We used the OG590+32 filter together with

[10] Observations conducted under ESO DDT programs 294.A-5018 and 294.A-5039; PI: D. Sobral.

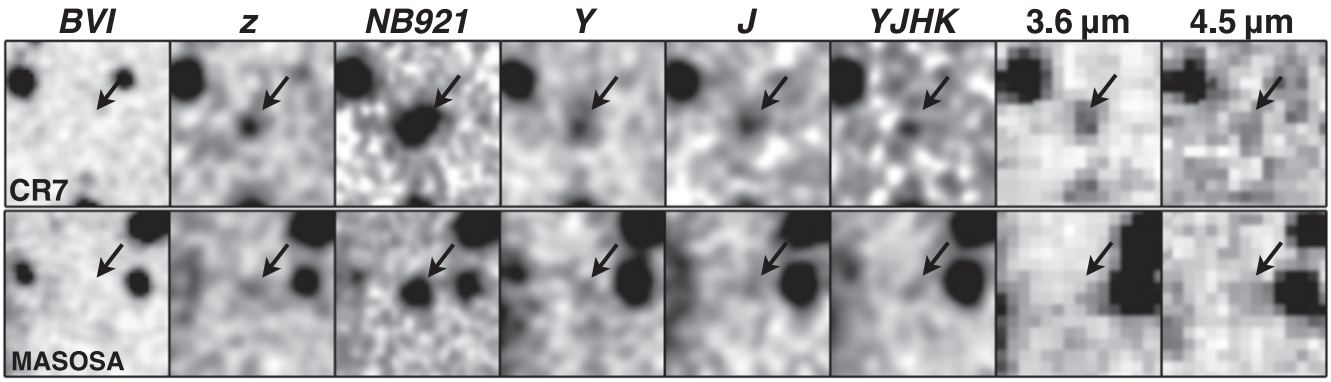

Figure 2. Thumbnails of both luminous Lyα emitters in the optical to MIR from left to right. Each thumbnail is $8 \times 8''$, corresponding to $\sim$44 × 44 kpc at $z \sim 6.6$. Note that while for MASOSA the Lyα emission line is detected by the NB921 filter at full transmission, for CR7 the Lyα is only detected at $\sim$50% transmission. Therefore, the NB921 only captures $\sim$50% of the Lyα flux: the observed flux coming from the source is $\sim$2× larger.

the GRIS300I+11 Grism (1.62 Å pix^{-1}) with the 1″ slit. Lyα is clearly seen in each individual exposure of 1 ks.

We use the ESO FORS2 pipeline to reduce the data, along with a combination of Python scripts to combine the 2D and extract the 1D. The steps implemented follow a similar procedure to that used for DEIMOS.

2.2.3. X-SHOOTER/VLT Observations

Our X-SHOOTER/VLT (Vernet et al. 2011) observations targeted "CR7" and were obtained on 2015 January 22 and February 15. The seeing varied between 0.″8 and 0.″9 and observations were done under clear conditions. We obtained individual exposures of 0.27 ks for the optical arm, while for NIR we used individual exposures of 0.11 ks. We nodded from an A to a B position, including a small jitter box in order to always expose on different pixels. We used 0.″9 slits for both the optical and NIR arms (resolution of $R \sim 7500$ and $R \sim 5300$, for the optical and NIR arms, respectively). In total, for the X-SHOOTER data, we obtained 8.1 ks in the optical and 9.9 ks in the NIR. The differences are driven by the slower read-out time in the optical CCD compared to the NIR detector.

We use the ESO X-SHOOTER pipeline to fully reduce the visible (optical) and NIR spectra separately. The final spectrum is shown in Figure 3.

2.2.4. SINFONI/VLT Observations

We have also observed CR7 with the SINFONI (Eisenhauer et al. 2003; Bonnet et al. 2004) integral field unit on the VLT on 2015 March 8, 11–13, 17, and April 4. The seeing varied between 0.″6 and 0.″9 (median: 0.″77) in the J band and observations were done under clear conditions. We used the non-adaptive optics mode (spaxel size: 0.″25, field of view of $8 \times 8''$) with the J-band grism ($R \sim 2000$) and individual exposure times of 0.3 ks. We took advantage of the relatively large spatial coverage to conduct our observations with a jitter box of 2″ (nine different positions for each set of 2.7 ks observations). We obtained 45 exposures of 0.3 ks each, resulting in a total exposure time of 13.5 ks.

We use the SINFONI pipeline (v2.5.2) in order to reduce the data. The SINFONI pipeline dark subtracts, extracts the slices, wavelength calibrates, flat-fields and sky-subtracts the data. Flux calibration for each observation was carried out using standard star observations which were taken immediately before or after the science frames. A final stacked data-cube is produced by co-adding reduced data from all the observations. The collapsed data-cube does not result in any continuum detection, as expected given the faint J flux. We extract the 1D spectrum using an aperture of 1″.

3. MEASUREMENTS AND SED FITTING

3.1. Redshifts

In both the VLT (FORS2 or X-SHOOTER) and Keck (DEIMOS) spectra for the two targets, we detect the very strong Lyα line (Figure 3) in emission, and no continuum either directly red-ward or blue-ward of Lyα. The very clear asymmetric profiles leave no doubts about them being Lyα and about the secure redshift (Figure 3). Particularly for CR7, the high signal-to-noise ratio (S/N) $>150\sigma$ (combined Keck and VLT) at Lyα, despite the very modest exposure time for such a high-redshift galaxy, clearly reveals that this source is unique.

Based on Lyα, we obtain redshifts of $z = 6.604$ for CR7[11] and $z = 6.541$ for MASOSA. The redshift determination yields the same answer for both our data sets: X-SHOOTER and DEIMOS, for CR7 and FORS2 and DEIMOS, for MASOSA (see Figure 3, which shows the agreement). It is worth noting that for CR7 we find that the Lyα emission line is detected in a lower transmission region of the NB921 filter profile (50% of peak transmission). Therefore, the Lyα luminosity of CR7 is higher than estimated from the NB921 photometry, making the source even more luminous than thought.

3.2. Spectral Line Measurements

By fitting a Gaussian profile to the emission lines, we measure the EW (lower limits, as no continuum is detected) and FWHM. Emission line fluxes are obtained by using NB921 and Y photometry (similarly to e.g., Ouchi et al. 2009, 2013), in combination with the NB921 filter profile and the appropriate redshift. We also check that the integrated emission line (without any assumption on the fitting function) provides results that are fully consistent.

For MASOSA, we find no other line in the optical spectrum, and also find no continuum at any wavelength probed (see Figure 3). For CR7, we find no continuum either directly blue-ward or red-ward of Lyα in the optical spectrum (both in X-SHOOTER and DEIMOS; Figure 3). However, we make a continuum detection (spatially very compact) in the rest-frame

[11] CR7 has a redshift of $z = 6.600$ based on He II 1640 Å (see Section 3.3).

Table 1
Sources and Observation Log

Source[a]	R.A. (J2000)	Decl. (J2000)	Int. Time VLT[b] [Keck] (ks/pixel)	Dates of Observations	Features Detected in Spectrum[c]
CR7	10 00 58.005	+01 48 15.251	VIS: 8.1, [5.4]	2014 Dec 28; 2015 Jan 22, Feb 15	916–1017 Å, Lyα, He II 1640 Å
CR7	10 00 58.005	+01 48 15.251	NIR: 9.9	2015 Jan 22, Feb 15	He II 1640 Å
CR7	10 00 58.005	+01 48 15.251	SINFONI: 13.5	2015 Mar 8, 11–13, 17 and 2015 Apr 4	He II 1640 Å
MASOSA	10 01 24.801	+02 31 45.340	VIS: 6, [2.7]	2014 Dec 29; 2015 Jan 12	Lyα

Notes.
[a] Observation log for the two luminous Lyα emitter candidates, observed with both the VLT (using X-SHOOTER and SINFONI: CR7 and FORS2: MASOSA) and Keck (using DEIMOS for both sources), which we have spectroscopically confirmed.
[b] Note that for X-SHOOTER (CR7) the VIS (visible) and NIR (near-infrared) arms provide different total exposure times (due to different read-out times), and we thus provide them separately in different lines. Keck/DEIMOS exposure times are presented between square brackets: [exposure time].
[c] We also note the features and lines detected in the spectra: for CR7 we detect rest-frame UV just redder of the Lyman-limit, with a clear Lyα forest, but such flux completely disappears toward redder wavelengths, implying a very blue spectra. No continuum is detected apart from that. An extremely luminous, high EW and narrow Lyα emission line is detected for each of the sources. For CR7, where we have NIR coverage, from both X-SHOOTER and SINFONI, we detect high EW He II 1640 Å emission fro both instruments, but no other lines.

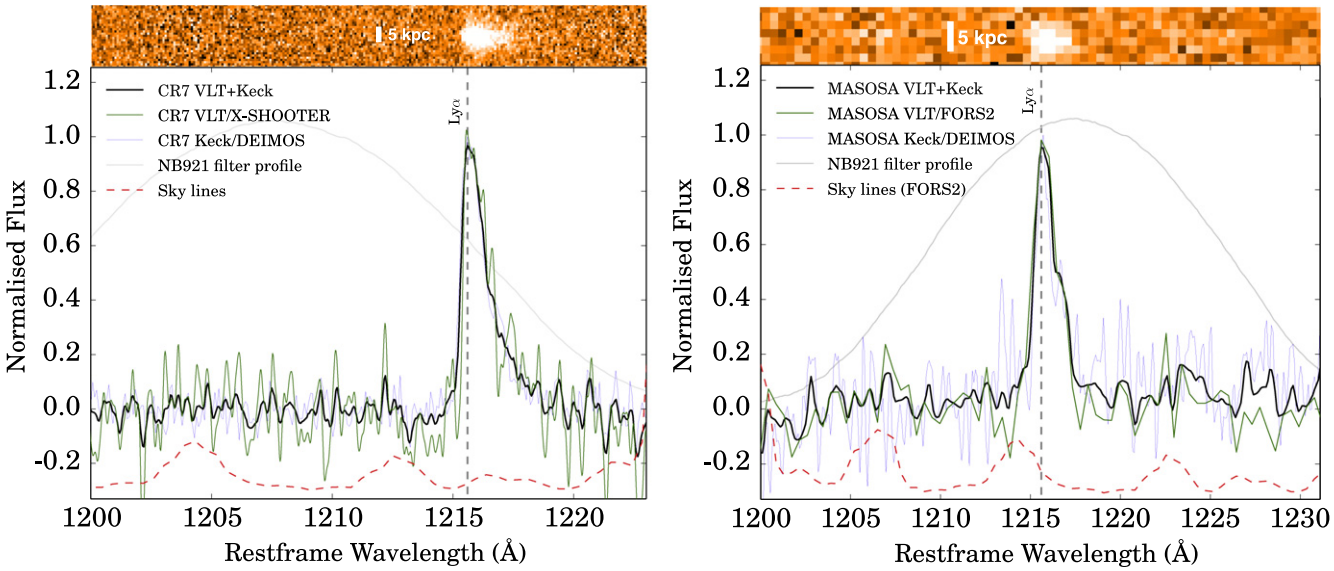

Figure 3. Left: "CR7" 1D and 2D optical spectra, showing the strong and clear Lyα emission line. We also show the NB921 filter profile which was used to select the source. Note that Lyα is detected at the wing of the NB921 filter. Thus, while the NB921 photometry already implied that the source was very luminous, its true luminosity was still underestimated by a factor of 2. We show both our Keck/DEIMOS and VLT/X-SHOOTER spectra, which show perfect agreement, but with X-SHOOTER providing an even higher spectral resolution, while the DEIMOS spectrum gives an even higher S/N. Right: "MASOSA" 1D and 2D optical spectra (FORS2), showing the strong and clear Lyα emission line. We also show the NB921 filter profile which was used to select the source. We show both the VLT/FORS2 and Keck/DEIMOS spectra, showing that they agree very well. The DEIMOS spectrum provides higher resolution, but both clearly reveal the asymmetry of the line, confirming it as Lyα without any doubt.

916–1017 Å for CR7 (rest-frame Lyman–Werner photons), with clear absorption features corresponding to the Lyα forest. The reddest wavelength for which we can see continuum directly from the spectra corresponds to Lyα at $z = 5.3$. For higher redshifts, the flux is consistent with zero for our spectra. This clear continuum detection at wavelengths slightly redder than the Lyman-limit, but then disappearing for longer wavelengths, can be explained by a combination of a very blue, strong continuum (intense Lyman–Werner radiation) and an average increase of the neutral hydrogen fraction along the line of sight toward higher redshift, similar to the Gunn-Peterson trough observed in quasar spectra (e.g., Becker et al. 2001; Meiksin 2005). However, due to the average transmission of the intergalactic medium (IGM), the fact that even just a fraction of the light is able to reach us is a unique finding. These findings will be investigated separately in greater detail in a future paper, including further follow-up which will allow an even higher S/N.

3.3. NIR Spectra of CR7: He II and no Other Lines

We explore our X-SHOOTER NIR spectra to look for any other emission lines in the spectrum of CR7. The photometry reveals a clear *J*-band excess (0.4 ± 0.13 mag brighter than expected from *Y*, *H* and *K*; see Table 2), which could potentially be explained by strong emission lines (e.g., C IV 1549 Å, He II 1640 Å, O III] 1661 Å, O III] 1666 Å, N III] 1750 Å).

We mask all regions for which the error spectrum is too large (>1.5× the error on OH line free regions), including the strongest OH lines. We then inspect the spectrum for any emission lines. We find an emission line at 12464 Å (see Figure 4). We find no other emission lines in the spectrum

Table 2
A Summary of Our Results for CR7 and MASOSA and Comparison to Himiko

Measurement[a]	CR7	MASOSA	Himiko
z_{spec} Lyα	$6.604^{+0.001}_{-0.003}$	6.541 ± 0.001	6.54
β UV slope	-2.3 ± 0.08	…	-2.0 ± 0.57
Lyα (FWHM, km s^{-1})	266 ± 15	386 ± 30	251 ± 21
Lyα (EW$_{0,obs,Y}$[b], Å)	211 ± 20	>206	78 ± 8
Lyα (EW$_{0,obs,spec}$, Å)	>230	>200	…
Lyα (Log$_{10}$ L, erg s^{-1})	43.93 ± 0.05	43.38 ± 0.06	43.40 ± 0.07[c]
Lyα/N v	>70	…	…
He II/Lyα	0.23 ± 0.10	…	…
He II (EW$_0$, Å)	80 ± 20 (>20)	…	…
He II (FWHM, km s^{-1})	130 ± 30	…	…
He II/O III] 1663	>3	…	…
He II/C III] 1908	>2.5	…	…
Photometry	**CR7**	**MASOSA**	**Himiko**
z	25.35 ± 0.20	26.28 ± 0.37	25.86 ± 0.20[d]
NB921 2″ aperture	23.70 ± 0.04	23.84 ± 0.04	23.95 ± 0.02[e]
NB921 MAG-AUTO	23.24 ± 0.03	23.81 ± 0.03	23.55 ± 0.05[d]
Y	24.92 ± 0.13	>26.35	25.0 ± 0.35[f]
J	24.62 ± 0.10	>26.15	25.03 ± 0.25[d]
H	25.08 ± 0.14	>25.85	25.5 ± 0.35[f]
K	25.15 ± 0.15	>25.65	24.77 ± 0.29[d]
3.6 μm	23.86 ± 0.17	>25.6	23.69 ± 0.09[d]
4.5 μm	24.52 ± 0.61	>25.1	24.28 ± 0.19[d]

Notes.
[a] These include both the spectroscopic measurements, but also photometry. In order to provide an easy comparison, we also provide the measurements for Himiko, the other luminous source in the Matthee et al. (2015) sample, fully presented in Ouchi et al. (2013). Note that the intrinsic Lyα properties may be significantly different from the observed ones, if there is significant absorption by the galaxies themselves.
[b] Using Y-band photometry to estimate the continuum.
[c] Recomputed by using Y band to estimate the continuum, in order to match our calculation for CR7 and MASOSA.
[d] Measurement from Ouchi et al. (2013).
[e] Measurement by Matthee et al. (2015) based on own UDS reduction.
[f] Measurement from Bowler et al. (2014) since the Y and H data has been significantly improved with the availability of new VISTA and UKIDSS data.

(Figure 4). The emission line found, at $z = 6.600$[12], corresponds to 1640 Å, and thus we associate it with He II. Given the line flux ($4.1 \pm 0.7 \times 10^{-17}$ erg s^{-1} cm^{-2}), and the level of continuum estimated from e.g., Y and H bands, the line flux we measure is sufficient to explain the J-band excess. It also means that we detect He II with a high rest-frame EW (>20 Å) with our X-SHOOTER spectra, consistent with the necessary rest-frame EW in order to produce the excess in the J band (~80 Å, reliably estimated from photometry). We find that the He II 1640 Å emission line is narrow (130 ± 30 km s^{-1} FWHM), and detected at 6 σ in our X-SHOOTER data. Results are presented in Table 2.

In order to further confirm the reality, strength and flux of the He II 1640 Å line, we also observed CR7 with SINFONI on the VLT. SINFONI reveals an emission line at the central position of CR7 (at the peak of Lyα emission), spatially compact (unresolved) and found at 12464 Å, thus matching our X-SHOOTER results. We co-add the X-SHOOTER and SINFONI spectra and show the results in Figure 4. When co-adding the spectra, we normalize both spectra at the peak value of He II 1640 Å and explicitly mask the strong OH lines.

Our He II 1640 Å emission line implies a small velocity offset between the peak of Lyα and He II 1640 Å of +160 km s^{-1} (i.e., the Lyα peak is redshifted by +160 km s^{-1} in respect to He II, which could also be interpreted as an outflow). This means that, not surprisingly, we are only detecting the red wing of the Lyα line, while both the blue wing and any potential Lyα component with <+160 km s^{-1} is being likely absorbed and cannot be observed. This may imply that the intrinsic Lyα flux or luminosity and the EW will be even larger than measured.

4. DISCOVERY OF THE MOST LUMINOUS LYα EMITTERS

4.1. MASOSA

MASOSA is particularly compact (0.″7 in diameter, corresponding to 3.8 kpc diameter at $z = 6.541$). It is similar to sources now found by MUSE (e.g., Bacon et al. 2014; Karman et al. 2015), that are completely undetected in the continuum and thus similar to typical Lyα emitters that have been found over the last years with e.g., Subaru/Suprime-cam. However, MASOSA is extremely bright in Lyα and thus separates it from the very faint sources found with MUSE in the HDF south and from other Lyα emitters. MASOSA is undetected in all continuum bands at all wavelengths and even the weak detection in z' can be fully explained by the luminous Lyα line and little to no continuum. The estimated rest-frame EW of the Lyα line from spectroscopy is very high (>200 Å), thus implying a likely very metal-poor stellar population (Malhotra & Rhoads 2002). Its nature is likely similar to other metal-poor Lyα emitters (Nagao et al. 2008; Ono et al. 2010, 2012). Given the very high EW and no continuum detection, MASOSA is likely extremely young, metal-poor and likely contains low stellar mass (<10^9 $M_\odot$).

The Lyα emission line shows a FWHM of 386 ± 30 km s^{-1}, and with tentative evidence for two components in the Lyα line (similar to what is found by Ouchi et al. 2010), potentially indicating a merger or radiative transfer effects (e.g., Verhamme et al. 2006). However, with the current ground-base imaging, and the faintness in the continuum, it is not possible to conclude anything about the potential merging nature of the source–only *HST* follow-up can investigate this. However, what is already clear is that MASOSA provides a new example of a relatively compact Lyα emitter with a similar luminosity to Himiko (Ouchi et al. 2009, 2013), but with a much more extreme EW, revealing that such high luminosity sources present diverse properties and may have a diverse nature.

4.2. CR7

CR7 clearly stands out as the most luminous Lyα emitter at $z \sim 7$, with a luminosity of $L_{Ly\alpha} = 10^{43.93 \pm 0.05}$ erg s^{-1}, ~3× more luminous than any known Lyα emitter within the epoch of reionization. It also presents a very high rest-frame EW of >200 Å, and thus a likely intrinsic EW which is even higher because of absorption by the ISM. Our measurements are presented in Table 2.

CR7 is spatially extended: 3″ in diameter, corresponding to ~15 kpc at $z = 6.6$, as seen from its narrow-band image, but

[12] The redshift measured from the He II 1640 Å emission line implies a small positive velocity offset between the peak of Lyα and He II 1640 Å of +160 km s^{-1}, i.e., the Lyα peak is redshifted by +160 km s^{-1} in respect to He II.

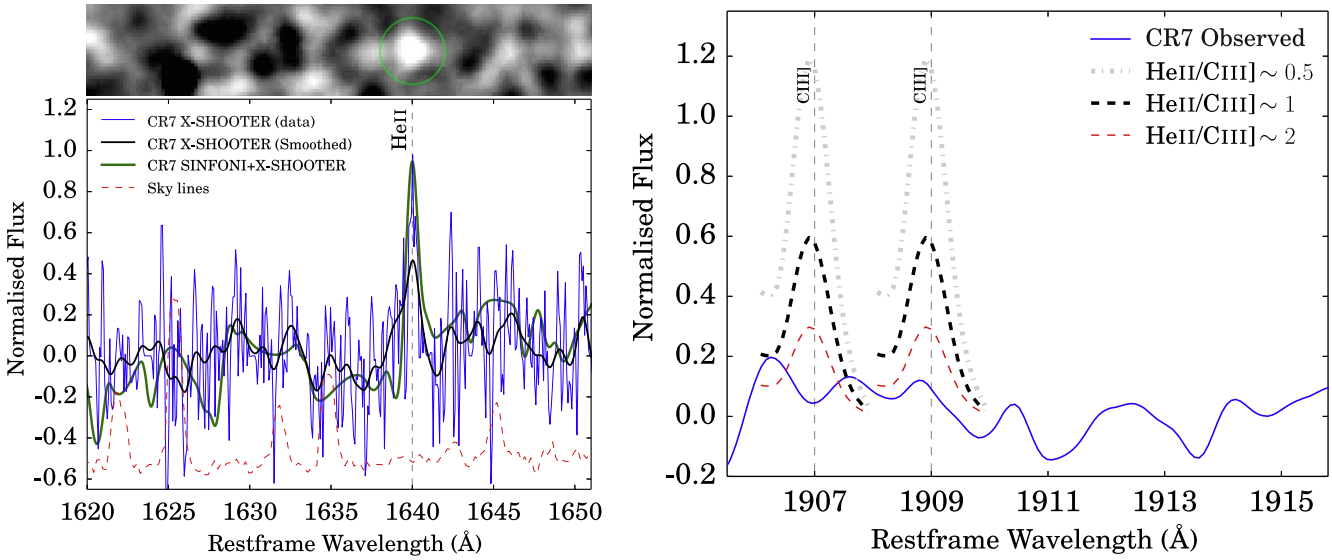

Figure 4. Left: our X-SHOOTER NIR spectrum of CR7, revealing a significant detection of the He II 1640 Å emission line. We show both the data at full resolution and binning in wavelength (with a resolution of 0.4 Å). We also show the combined X-SHOOTER and SINFONI data and also show the sky spectrum. We note that sky lines were explicitly masked, but some residuals are still visible, including those of two OH lines just redder of the He II emission line, which show up as a slight flux increase and another one bluer of He II, which has been slightly over-subtracted. We note that no continuum is found in the NIR spectra, and that we would require significantly deeper observations in order to detect it simply based on the NIR photometry. Right: we investigate the NIR X-SHOOTER spectrum for other emission lines (e.g., Stark et al. 2014). We do not find any other emission line apart from He II, but we show one of the lines that should be stronger in our spectrum (typically ∼2× stronger than He II, thus He II/C III] ∼ 0.5). We use our He II line detection and show it at the position of the C III] doublet for a typical line ratio of He II/C III] of 0.5, but also a line ratio of ∼1 and ∼2. Our data allow us to place a limit of He II/C III] > 2.5. We also investigate the presence of N V 1240, N IV 1487, C IV 1549, O III] 1661, O III] 1666, N III] 1750: all of these are undetected.

also in the spectra. Both the X-SHOOTER and DEIMOS data confirm its spatial extent, with both of them agreeing perfectly on the redshift, extent and FWHM. While the Lyα line profile is narrow (FWHM $\approx$ 270 km s^{-1}), and particularly for such high luminosity, we see evidence for potentially 2 or 3 components (double peaked Lyα emission and a redshifted component toward the south of the source) and/or signs of absorption (see Figure 3), which indicate a complex dynamical structure. It may also mean that the actual intrinsic FWHM is even narrower. However, such tentative evidence requires confirmation with further spectroscopy obtained over different angles, and particularly by exploring deep imaging with high enough spatial resolution with e.g., *HST*.

4.3. Comparison with Himiko

We find that CR7 may be seen as similar to Himiko (but much brighter in Lyα and much higher EW) due to both sources presenting a spatial extent of about 3″ in diameter. Both could therefore be tentatively classed as Lyα "blobs" (e.g., Steidel et al. 2000, 2011; Matsuda et al. 2004). However, we note that Himiko is detected at peak transmission in the NB and the NB imaging in which it is detected is 1 mag deeper (see Matthee et al. 2015) than the imaging used for the discovery of CR7. While the CR7 Lyα line profile is very narrow, it consists of 2 or potentially 3 components, which may indicate that the source is a double or triple merger, likely similar to Himiko in that respect as well (see Section 5.4 which shows this is very likely the case for CR7). However, a simpler explanation is radiation transfer, which can easily cause such bumps (e.g., Vanzella et al. 2010). There are other similarities to Himiko, including: detections in NIR and a blue IRAC color. CR7 is however a factor ∼3 brighter in Lyα emission and has an excess in J band (attributed to He II emission). CR7 is also bluer ($\beta = -2.3 \pm 0.08$, either using $Y-H$ or $H-$K, following Equation (1) of Ono et al. 2010) in the rest-frame UV when compared to Himiko (which shows $\beta \sim -2.0$, but note that Himiko shows a red color from H to K which would imply $\beta \sim 0.2$ if those bands are used). Furthermore, while for CR7 we see some rest-frame UV light just redder of the Lyman-limit, corresponding to Lyman–Werner radiation (very compact, coincident with the peak of Lyα emission and the *HST* detection), this is not seen at all for Himiko (Zabl et al. 2015). Also, while CR7 shows a strong He II 1640 Å emission line, no He II is detected in Himiko, even though Zabl et al. (2015) obtained very deep X-SHOOTER data.

MASOSA is quite different. While it has the highest Lyα peak brightness, it is not extended and not detected in NIR or IRAC. Therefore, MASOSA provides also a new class of sources at the epoch of reionization: as luminous as Himiko, but very compact and with no significant rest-frame UV or rest-frame optical detection at the current UltraVISTA depth.

5. SED FITTING AND MODEL ASSUMPTIONS

To interpret the photometry/SED of CR7 we exploit the SED-fitting code of Schaerer & de Barros (2009, 2010), which is based on a version of the *Hyperz* photometric redshift code of Bolzonella et al. (2000), modified to take nebular emission into account. We have explored a variety of spectral templates including those from the GALAXEV synthesis models of Bruzual & Charlot (2003), covering different metallicities (solar, $Z_\odot$, to 1/200 $Z_\odot$) and star formation histories (bursts, exponentially declining, exponentially rising). A standard IMF with a Salpeter slope from 0.1 to 100 $M_\odot$ is assumed. We refer to these models as "standard"/"enriched" SED fits or "standard"/"enriched" models throughout this paper.

In addition, we also use synthetic spectra from metal-free (PopIII) stellar populations assuming different IMFs (Salpeter, top-heavy), taken from Schaerer (2002, 2003). Constant star

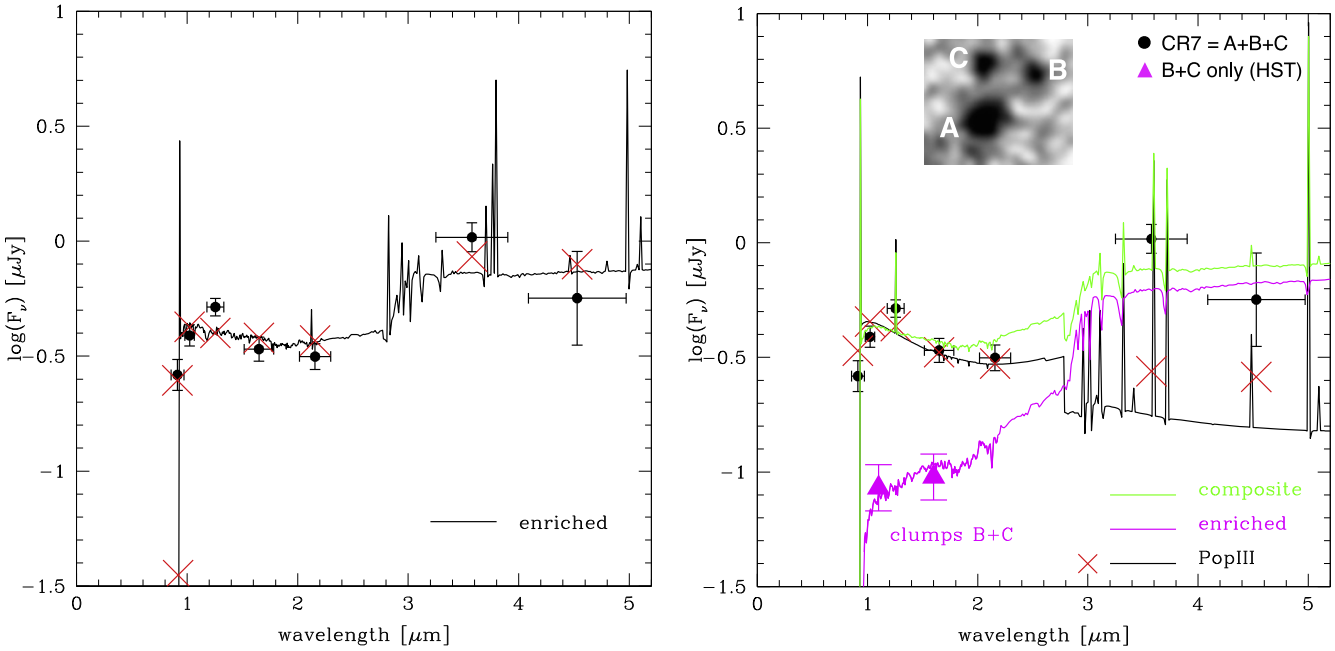

Figure 5. Left: the SED of "CR7," from observed optical (rest-frame FUV) to observed MIR (rest-frame optical) and the best fit with a normal stellar population (not including PopIII stars). Red crosses indicate the flux predicted for each broadband filter for the best fit. The fit fails to reproduce the strong Lyα emission line and also the excess in *J* band, due to He II emission. Moreover, and even though the fit is unable to reproduce all the information available for the source, it requires an age of 700 Myr (the age of the Universe is 800 Myr at $z = 6.6$). In this case, the galaxy would have an SFR of $\sim$25 $M_\odot$ yr^{-1} and a stellar mass of $\sim 10^{10.3}$ $M_\odot$. This, of course, is not able to explain the strong Lyα and the strong He II emission line. Right: same observed SED of CR7 as in the left panel plus *HST* photometry for clumps B+C (magenta triangles). The black line shows a fit with a pure PopIII SED to the rest-frame UV part; the magenta line the SED of an old simple stellar population with 1/5 solar metallicity which matches the flux from clumps B+C; the green line shows the predicted SED summing the two populations after rescaling the PopIII SED by a factor of 0.8. The composite SED reproduces well the observed photometry. Although there is tension between the strength of the He II line and nebular continuum emission (cf. text), a PopIII contribution is required to explain the He II λ1640 line and the corresponding excess in the *J* band. Although He II is very strong, we find no evidence for any other emission lines that would be characteristic of an AGN. Furthermore, the clear IRAC detections and colors, and particularly when taken as a whole, can be fully explained by a PopIII population, while a normal stellar population or an AGN is simply not able to.

formation rate (SFR) or bursts are explored in this case. We also explore SEDs from "composite" stellar populations, showing a superposition/mix of PopIII and more normal populations.

Nebular emission from continuum processes and emission lines are added to the spectra predicted as described in Schaerer & de Barros (2009). Nebular emission from continuum processes and emission lines are proportional to the Lyman continuum photon production. Whereas many emission lines are included in general, we only include H and He lines for the PopIII case (cf. Schaerer 2003). The IGM is treated with the prescription of Madau (1995). Attenuation by dust is described by the Calzetti law (Calzetti et al. 2000).

5.1. CR7: SED Fitting with a Normal Population

Part of the photometry of CR7 is explained relatively well with "standard" models, as illustrated in Figure 5 (left panel). The shortcomings of these fits is that they cannot account for the relative excess in the *J* band with respect to *Y*, *H*, and *K*, and that the Lyα emission is not strong enough to reproduce the entire flux observed in the NB921 filter. Both of these shortcomings thus relate to the presence of the strong emission lines (Lyα and He II) observed in spectroscopy and also affecting the broadband photometry.

The typical physical parameters derived from these SED fits which only include "normal" stellar populations indicate a stellar mass $M_* \sim 2 \times 10^{10}\,M_\odot$, SFR $\sim$ 25 $M_\odot$ yr^{-1}, and a fairly old age ($\sim$700 Myr; the universe is $\sim$800 Myr old at $z = 6.6$). The SED fits and the derived parameters do not vary much for different star formation histories (SFHs): both for exponentially declining and rising cases, the fits prefer long timescales (i.e., slowly varying SFHs). Whereas for exponentially declining SFHs and for constant SFR the best-fit attenuation is negligible ($A_V = 0$), a higher attenuation is needed for rising SFHs, as expected (cf. Schaerer & Pelló 2005; Finlator et al. 2007). Depending on the assumed metallicity, this may reach from $A_V = 0.5$ (for 1/5 solar) to 0.25 (for 1/200 $Z_\odot$). The corresponding SFR is $\sim$30–40 $M_\odot$ yr^{-1}, and the predicted IR luminosity ranges from $\log(L_{\rm IR}/L_\odot) = 10.4$ to 11.2, assuming energy conservation. The typical specific SFR, sSFR, obtained from these fits is sSFR $\sim$ 1.2–1.9 Gyr^{-1}, as expected for a "mature" stellar population with SFH close to constant (c.f. González et al. 2014).

5.2. CR7: SED Fitting with Contribution from PopIII Stars

The presence of strong Lyα and He II emission lines, plus the absence of other UV metal emission lines (cf. above), may be due to exceptionally hot stars with a strong and hard ionizing flux, resembling that expected for PopIII stars (cf. Tumlinson et al. 2001; Schaerer 2002). A fit with PopIII templates (from Schaerer 2002, 2003) is shown in Figure 5 (right panel: black line). PopIII models (Schaerer 2002, 2003) show that at 3.6 μm (for $z = 6.6$) there are strong He II and He I lines, apart from Hβ, and that these Helium emission lines should have fluxes comparable to that of Hβ in the case of PopIII (Schaerer 2002). Specifically, 3.6 μm should be contaminated by He II 4686, He I 4471 and He I 5016. For 4.5 μm, apart from Hα, the He I 5876 should be detected and could be comparable to Hβ. The general

features of our fits with PopIII templates (considering bursts or constant SFR, as well as different IMFs) are the following.

1. The UV rest-frame part of the SED is very well reproduced, allowing naturally for a "boost" of the *J*-band flux due to the presence of the He II line and for a stronger Lyα line due to a higher Lyman continuum flux (for the same UV flux). The exact strength of these emission lines is very sensitive to the "details" of the population, such as the upper end of the IMF, the age or star formation history (see more details in, e.g., Raiter et al. 2010). The fits with PopIII also reproduce all other NIR detections: *Y*, *H*, and *K* (see Figure 5).
2. Populations with very strong line-emission also have a strong nebular continuum emission red-ward of Lyα and increasing toward the Balmer limit (see, e.g., Schaerer 2002). The observations (*H*- and *K*-band photometry) do not permit a much stronger contribution from the nebular continuum, as that would mean an increasing redder $H-K$ color, which is not observed. This limits the maximum strength of the predicted emission lines, except if the two emission processes (recombination line emission and nebular continuum emission, which is due to two-photon and free-bound emission) could be decoupled, and emission lines could be increased without significantly increasing the nebular continuum emission.
3. All the available PopIII templates fitting the (rest-)UV part of the spectrum, predict a relatively low flux in the IRAC bands with or without accounting for emission lines. Therefore, a pure metal-free population does not seem to be able to completely reproduce the observed rest frame UV–optical SED of this source. In any case, a PopIII only explanation would not seem very likely. Therefore, a metal-free population alone (without decoupling between recombination line emission and nebular continuum emission) is not able to reproduce the observed rest-frame UV–optical SED of this source.

5.3. PopIII and a More Chemically Evolved Stellar Population

As a consequence of our findings, we are led to consider a hybrid SED consisting of two populations (the source may well be a merger, and these components may well be completely separated, avoiding pollution by metals into the potentially metal-free region): a young metal-free stellar population and a more chemically evolved population. This can be fully confirmed by using *HST* and appropriate filters that can easily isolate Lyα, the rest-frame UV, and He II.

A superposition of a young PopIII component dominating in the UV and an older population of "normal" metallicity (in this case, $0.2\,Z_{\odot}$) dominating the rest-frame optical flux of CR7 is shown in the right panel of Figure 5. In practice, we add 80% of a metal-free simple stellar population with an age of 16 Myr (shown by the black line; although younger ages of $\lesssim$5 Myr are preferred to produce the strongest He II emission) to a 360 Myr old burst of $1/5\,Z_{\odot}$ (magenta curve), giving the total flux shown in green. As can be seen, an "old" population of $\sim 1.6\times10^{10}\,M_{\odot}$ can make up for the missing rest-frame optical flux, whereas a young PopIII burst can dominate the UV and the emission lines. There is some tension/uncertainty in the age or age spread of the metal-free population, as very young ages ($\lesssim$5 Myr) are preferred to produce the strongest He II emission, whereas slightly older ages are preferred to avoid too strong nebular continuum emission (cf. above). For indication, the mass of the metal-free component would be $1.4\times10^{9}\,M_{\odot}$ for a Salpeter IMF from 1 to $500\,M_{\odot}$, i.e., ~9% of mass of the old population. However, significantly less mass could be needed if the PopIII IMF was flat or top-heavy, lacking e.g., completely low mass stars (stars below $10\,M_{\odot}$). This could mean that $\sim10^{7}\,M_{\odot}$ of PopIII stars would be needed in order to fully explain the flux for an IMF peaking at $\sim60\,M_{\odot}$, or even less if the IMF peaks at even higher masses. This reveals that the presence of a young, metal-free population, forming for example in a yet un-polluted region of the galaxy, in an slightly evolved galaxy at $z = 6.6$, could reproduce the observed features of CR7 (consistent with theoretical predictions from e.g., Scannapieco et al. 2003; Tornatore et al. 2007).

5.4. HST Imaging of CR7

In order for our best interpretation to be valid, CR7 would require to be clearly separated/resolved, with *HST* resolution, into at least two different spatial components: one being dominated by a PopIII-like stellar population (dominating the UV light but with only a very small fraction of the mass), and another, redder in the UV (and fully dominating the mass), with fluxes similar to those shown in Figure 5. While this requires more detailed follow-up, we find that CR7 has been fortuitously observed and is in the field of view of previous WFC3 observations in F110W (broad *YJ* filter that also contains Lyα) and F160W (*H*) of a different project (ID: 12578, PI: Forster-Schreiber). We explore such data in order to investigate the rest-frame UV morphology of CR7 and to conduct a first study of the rest-frame UV colors. Observations in F110W and F160W were obtained for 2.6 ks each.

We show the data in Figure 6, including a comparison with out NB921 imaging. Figure 7 presents a false-color image combining data obtained with NB921, F110W and F160W. We find that CR7 is, beyond any doubt, split in different components (see Figures 6 and 7), in line with our best interpretation of a PopIII-like stellar population which dominates the UV, and a redder stellar population, found to be physically separated by at least 5 kpc (projected). In fact, we actually find three different components, which we label as A, B and C (see Figures 6 and 7). We obtain photometry for each of the clumps separately, in order to quantitatively test if they could explain the UV photometry predicted for the two components in Section 5.3. We use $0\farcs4$ apertures for components B and C and $1''$ for component A, more spatially extended.

We find that the sum of the two redder, fainter clumps (B +C) matches our evolved stellar population remarkably well (see Figures 5 and 8). Note that the photometry of the two redder clumps was not used to derive such fit. We find that the central clump (A) is the one that dominates the rest-frame UV light (Figure 8). Figure 7 also shows the rest-frame colors of components A, B and C. We also find that the peak of He II emission line (from SINFONI, although with low spatial S/N) and the peak of Lyα (high S/N but extended) likely originate (within the errors) from the center of the brightest UV clump (A). The clumps are physically separated by ~5 kpc.

The *HST* imaging reveals that CR7 may be either a triple merger (similar to Himiko), and/or a system where we are witnessing a PopIII star formation wave, which may have moved from the reddest clump (C) to the other (B) and we are observing the brightest UV clump at the right time (A). We

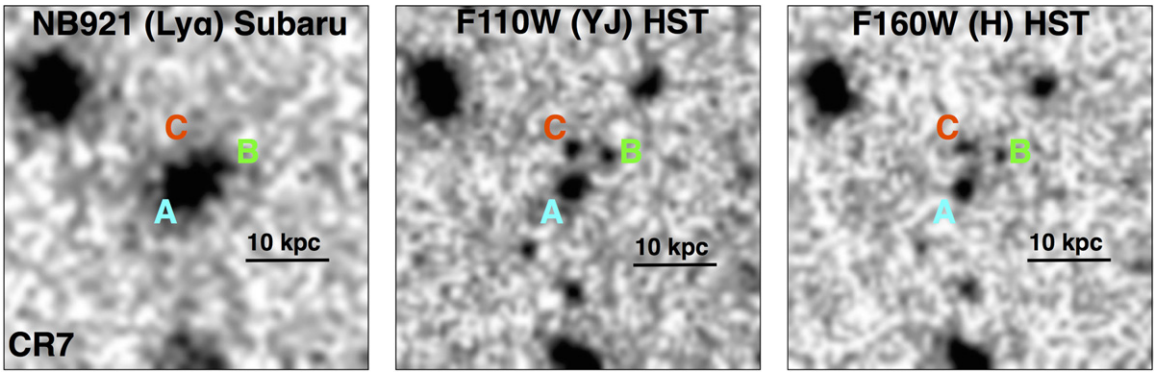

Figure 6. Left: CR7 with the NB921 filter/Suprime-cam imaging on Subaru, showing the extent of the Lyα but note that NB921 detects Lyα at only 50% transmission. Middle: *HST* imaging in *YJ*, revealing that CR7 clearly splits into three different components which we name A, B, and C. Right: *HST* imaging in *H*, again revealing the three different components in CR7. We find that component A fully dominates the rest-frame UV and is coincident with the peak of Lyα emission and the location at which we detect strong He II 1640 Å emission. Clumps B and C are much redder, and fully consistent with significantly contributing to the IRAC photometry. Note that because of the colors of the B and C clumps, they completely dominate the mass of the system, and thus the actual mass center of the system would be located between C and B, and significantly away from A. This is fully consistent with a scenario in with PopIII star formation is propagated in a wave from the central position toward the outskirts.

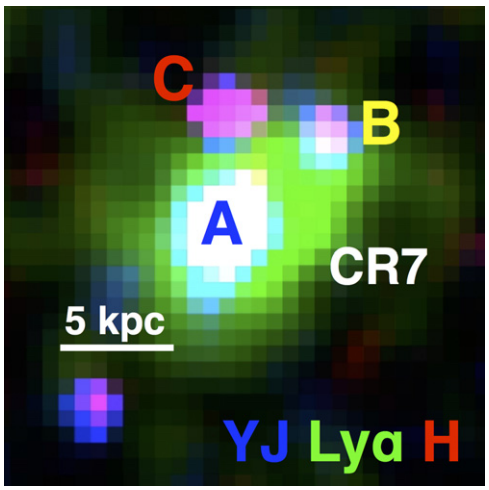

Figure 7. False color composite of CR7 by using NB921/Suprime-cam imaging (Lyα) and two *HST*/WFC3 filters: F110W (*YJ*) and F160W (*H*). This shows that while component A is the one that dominates the Lyα emission and the rest-frame UV light, the (likely) scattered Lyα emission seems to extend all the way to B and part of C, likely indicating a significant amount of gas in the system. Note that the reddest (in rest-frame UV) clump is C, with B having a more intermediate color and with A being very blue in the rest-frame UV.

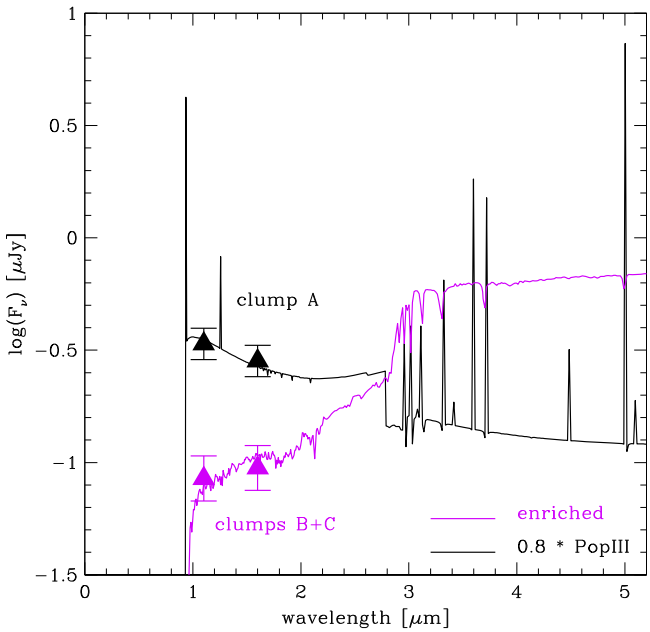

Figure 8. *HST* imaging in *YJ* and *H* allows us to physically separate CR7 into two very different stellar populations and shows remarkable agreement with our best-fit composite SED derived in Section 5.3. While clump A (see, e.g., Figure 7) is very blue and dominates the rest-frame UV flux, B+C are red and likely dominate the rest-frame optical and the mass. Note that the we simply show the *HST* data together with our best fit composite model derived in Section 5.3 which was solely based on the full photometry and did not make use of any resolved *HST* data.

have direct evidence of the intense Lyman–Werner radiation (rest-frame 912–1000 Å) from the brightest UV clump. It is therefore possible that the other clumps have emitted as much or even more of such radiation a few ~100 Myr before, preventing what is now the site of young massive stars (A) to form before and potentially allowing for that pocket of metal free gas to remain metal free. There are of course, other potential interpretations of our observations. In Section 6 we discuss the different potential scenarios in detail.

6. DISCUSSION

6.1. The Nature of CR7

CR7, with a luminosity of $L_{\mathrm{Ly}\alpha} = 10^{43.93\pm0.05}$ erg s^{-1} is ~3× more luminous than any known Lyα emitter within the epoch of reionization (e.g., Ouchi et al. 2013).

Our optical spectrum shows that the source is very blue toward the extreme ultra-violet up to the Lyman limit at 912 Å rest-frame, as we detect some faint continuum (spatially very compact) at rest-frame ~916–1017 Å (Lyman–Werner radiation). X-SHOOTER data also provides a NIR spectrum, allowing to investigate the significant excess seen in the *J*-band photometry from UltraVISTA (McCracken et al. 2012; Bowler et al. 2014), indicative of emission line(s). No continuum is detected in the NIR spectrum. However, and despite the relatively low integration time, a strong He II 1640 Å line was found (~6σ), capable of explaining the excess in the *J* band (see Figure 5). He II can only be produced if the intrinsic extreme UV spectrum is very hard, i.e., emits a large number of ionizing photons with energies above 54.4 eV, capable of

ionizing He completely. From our X-SHOOTER spectra, we place a lower limit in the rest-frame EW of the He II line of >20 Å, but estimate from photometry that the line has $EW_0 = 80 \pm 20$ Å, consistent with our spectroscopic lower limit. The line we detect is also narrower than Lyα, with FWHM of $130 \pm 30\,km\,s^{-1}$, as He II 1640 Å does not scatter easily as Lyα, as the line is not self-resonant.

While in principle there are a variety of processes that could produce both high EW Lyα and He II 1640 Å, some of them are very unlikely to produce them at the luminosities we are observing, such as X-ray binaries or shocks. However, in principle, cooling radiation could produce strong Lyα emission with luminosities similar to those measured for CR7. Faucher-Giguère et al. (2010) provides predictions of the total Lyα cooling luminosity as a function of halo mass and redshift. Under the most optimistic/extreme assumptions, it would be possible to produce a Lyα luminosity of $\sim 10^{44}\,erg\,s^{-1}$ for a dark matter halo mass of $M > 5 \times 10^{11}\,M_{\odot}$. Since such dark matter haloes should have a co-moving number density of about $\sim 10^{-5}\,Mpc^{-3}$ at $z \sim 6.6$, their number densities could potentially match the luminous Lyα emitters that we have found. However, in the case of cooling radiation, the He II emission line should be significantly weaker than what we measure (with intrinsic He II/Lyα of 0.1 at most; e.g., Yang et al. 2006), and cooling radiation in a massive dark matter halo should also result in a broader Lyα line than what we observe.

There are, nonetheless, four main sources known to emit an ionizing spectrum that can produce high luminosity, high EW nebular Lyα and He II as seen in our spectra (see also similar discussion in e.g., Prescott et al. 2009; Cai et al. 2011; Kashikawa et al. 2012).

(1) Strong AGNs (many examples have been found, particularly on, e.g., radio galaxies: De Breuck et al. 2000), with typical FWHM of lines being $\sim 1000\,km\,s^{-1}$.

(2) Wolf–Rayet (WR) stars (many cases known in e.g., SDSS: Shirazi & Brinchmann 2012; or see Erb et al. 2010 for a higher redshift example), with typical FWHM of lines being $\sim 3000\,km\,s^{-1}$.

(3) Direct collapse black hole (DCBH), which have been predicted and studied theoretically (e.g., Agarwal et al. 2013, 2015), although none has been identified yet, but they should produce strong He II 1640 Å (Johnson et al. 2011).

(4) PopIII stars (e.g., Schaerer 2003; Raiter et al. 2010), which should produce high EW, narrow He II emission lines (FWHM of a few $\sim 100\,km\,s^{-1}$).

Many potential candidates for PopIII have been identified based on their colors and/or high EW Lyα, but either no He II was found (e.g., Nagao et al. 2008), He II was found but with clear signatures of AGN activity (De Breuck et al. 2000; Matsuoka et al. 2009), or He II had very low EW (Cassata et al. 2013). Thus, so far, not a single source has been found with high EW Lyα, He II detection with high EW, no AGN signatures, no WR star signatures (e.g., P-Cygni profiles, broad lines, and many other metal lines e.g., Brinchmann et al. 2008; see also Gräfener & Vink 2015) and with no other metal lines.

6.2. The Nature of CR7: AGN or WR Stars?

In order to test the possibility of CR7 being an AGN, we start by checking X-ray data. We find no detection in the X-rays, with a limit of $<10^{44}\,erg\,s^{-1}$ (Elvis et al. 2009). We also find no radio emission, although the limit is much less stringent than the X-ray emission. The X-SHOOTER and DEIMOS spectra were carefully investigated for any metal lines, particularly N v, Oxygen and Carbon lines (see Table 2 and also Figure 4). No such lines were found, and thus we place 1σ upper limits on their fluxes, to constrain the nature of the source, finding, e.g., Lyα/N v > 70. Our Lyα and He II emission lines are narrow (both FWHM $\sim 100 - 300\,km\,s^{1}$), thus excluding broad-line AGN. Narrow-line AGNs with He II emission typically have C III] 1909/He II $\sim 1.5 \pm 0.5$ (e.g., De Breuck et al. 2000); such line ratio would result in a strong C III] 1909 detection in our X-SHOOTER spectrum (see Figure 4). We do not detect C III] 1909 and obtain a strong upper limit of C III] 1909/He II < 0.4 (1σ; see Figure 4), which greatly disfavors the AGN hypothesis. The strong limit on Lyα/N v > 70 also disfavors the AGN hypothesis and points toward very low metallicities.

There are no indications of WR stars, due to the very narrow He II line ($\sim 100\,km\,s^{-1}$, compared to typical FWHM of $\sim 3000\,km\,s^{-1}$ for WR stars, c.f. Brinchmann et al. 2008) and no other metal lines.

We note, nonetheless, that while CR7 is strongly disfavored as an AGN, it shows characteristics of what has been predicted for a DCBH (e.g., Johnson et al. 2011; Agarwal et al. 2013, 2015). This is because it shows $\beta = -2.3$ (as predicted), no metal lines, and high luminosity. The detection of the other nearby sources about ~5 kpc away (see Figure 6) are also a key prediction from Agarwal et al. (2015), while the relatively high observed He II/Lyα would also match predictions for a DCBH (Johnson et al. 2011). However, CR7 does not show any broad line, as predicted by Agarwal et al. (2013), and the observed Lyα and He II luminosities are higher by about ~2 orders of magnitude when compared to predictions by e.g., Johnson et al. (2011) for the case of $\sim 1\text{–}5 \times 10^4\,M_{\odot}$ black holes. Another key distinction between a DCBH and stellar population(s) is X-ray emission: if it is a black hole, it must be emitting much more X-ray flux than a PopIII stellar population, and thus would likely be detectable with *Chandra* given the high line luminosities measured. Deeper *Chandra* observations could in principle test this.

6.3. On the Hardness of the Ionizing Source of CR7

The theory of recombination lines relates, to first order, the ratio of He II to hydrogen recombination lines to the ratio between the ionizing photon flux above 54 eV, $Q(He^+)$, and that above 13.6 eV, $Q(H)$, the energies needed to ionize He^+ and H respectively. For the relative intensity He II λ1640/Lyα one thus has:

$$I(1640)/I(\mathrm{Ly}\alpha) \approx 0.55 \times \frac{Q\left(He^+\right)}{Q(H)}, \quad (1)$$

where the numerical factor depends somewhat on the electron temperature, here taken to be $T_e = 30$ kK (Schaerer 2002). The observed line ratio He II λ1640/Ly$\alpha \approx 0.22$ therefore translates to $Q(He^+)/Q(H) \approx 0.42$, which indicates a very hard ionizing spectrum. For metal-free stellar atmospheres such a hardness is only achieved in stars with very high effective temperatures, typically $T_{eff} > 140$ kK (or >100 kK for 1σ lower limit), hotter than the (already hot) zero-age main sequence predicted for PopIII stars which asymptotes to $T_{eff} \approx 100$ kK for the most massive stars (cf. Schaerer 2002). For integrated stellar populations consisting of a ensemble of stars of different

masses, a maximum hardness $Q(\mathrm{He}^+)/Q(\mathrm{H}) \approx 0.1$ is expected for zero or very low metallicities (Schaerer 2002, 2003), higher than inferred from the observed He II λ1640/Lyα ratio of CR7. This could indicate that only a fraction of the intrinsic Lyα emission is observed, or that a source with a spectrum other than predicted by the above PopIII models (e.g., an AGN) is responsible for the ionization or contributing at high energies (>54 eV). In fact the observed He II λ1640 EW of 80 $\pm$ 20 Å is in good agreement with the maximum EW predicted for PopIII models (Schaerer 2002). This supports the explanation that ~75% of the intrinsic Lyα emission may have escaped our observation, e.g.due to scattering by the IGM, internal absorption by dust, or due to a low surface brightness halo, processes which are known to affect in general Lyα emission (e.g., Atek et al. 2008; Dijkstra et al. 2011; Steidel et al. 2011). If the intrinsic Lyα emission is $\gtrsim$3–4 times higher than observed, the hardness ratio is compatible with "standard" PopIII models. Future observations and detailed photoionization models may yield further insight on the properties of the ionizing source of CR7.

6.4. CR7: A PopIII-like Stellar Population?

As the AGN and WR stars hypothesis are strongly disfavored (although we note that a DCBH could still explain most of our observations), could CR7 be dominated by a PopIII-like stellar population? For this to be the case, such stellar population would have to explain the detection, FWHMs, EWs and fluxes of Lyα and He II (including the strong excess in J band), the UV continuum and continuum slope ($\beta = -2.3 \pm 0.08$) and the IRAC detections which imply very high EW rest-frame optical lines. We have shown in Sections 5.3 and 5.4 that a composite of PopIII models (Schaerer 2002, 2003; Raiter et al. 2010) with a more evolved stellar population can match all our observations, including spatially resolved *HST* data. We note that the intrinsic He II/Lyα line ratio predicted for PopIII would be ~0.05–0.1 (Schaerer 2002, 2003), but that can easily result in an observable ratio of ~0.2–0.3 if a significant fraction of the Lyα line is absorbed/attenuated by neutral hydrogen. Since we find a velocity offset between He II and Lyα, our observations would support a an intrinsic He II/Lyα line ratio much closer to ~0.05–0.1, thus strongly favoring a PopIII-like population.

A key question, of course, is whether it is even possible or expected to observe Lyα coming from PopIII stars alone, even if such line is ultra-luminous. The most massive PopIII stars should be short-lived (a few Myr), and, without any previous contribution to ionize their surroundings from e.g., neighbor star clusters or other nearby proto-galaxies, the most massive PopIII stars would have to be able to emit enough ionizing photons to produce an ionized sphere larger than 1 Mpc after less than a few Myrs (Cen & Haiman 2000), before the most massive stars reach the supernovae phase and likely start enriching the local environment. However, such process (for a single PopIII population in full isolation, and fully surrounded by neutral hydrogen) should take at least ~3 Myr to happen: this is simply set by the speed of light. However, if neighboring sources (either PopIII or PopII stars) have already contributed toward ionizing a local bubble, and if PopIII star formation can proceed in a wave-like pattern, likely from the highest density regions to the lowest densities, by the time later PopIII stars form (still in pristine gas which was not contaminated due to being sufficiently far away), they will be in ideal conditions to be directly observed in Lyα. Thus, it may be much more likely to observe potentially composite populations than to observe pure PopIII stellar populations. Furthermore, and despite the nature of the stellar populations, it is likely that the observability of very luminous Lyα emitters is strongly favored in complex systems which already have older stellar populations like CR7 (that were able to ionize local bubbles before and thus allowing for strong Lyα emission from young stellar populations to be observable).

The detection of the signatures from the first generation of stars would provide the first glimpse into the general properties of these stars, such as their IMF. The mass of stars is a fundamental property, as it determines the evolution, the chemical enrichment of their surroundings and their faith. Theoretical work predicts that the first generation of stars are very massive, up to 1000 $M_\odot$ (Bromm & Larson 2004). More recent work is aiming to begin to sample the potential IMF of PopIII stars, finding a distribution which is very flat or top-heavy, with masses ranging from 10 to 1000 $M_\odot$ (e.g., Hirano et al. 2014), although the PopIII IMF is extremely uncertain (e.g., Greif et al. 2011) and only observations will be able to constrain it.

7. CONCLUSIONS

We presented the spectroscopic follow-up of the two most luminous $z \sim 6.6$ Lyα candidates in the COSMOS field ($L_{\mathrm{Ly}\alpha} \sim 3-9 \times 10^{43}$ erg s^{-1}): "MASOSA" and "CR7." These sources were identified in Matthee et al. (2015), revealing that such luminous sources are much more common than previously thought and have number densities of $\sim 1.5 \times 10^{-5}$ Mpc^{-3}. Our main results are as follows.

1. We used X-SHOOTER, SINFONI, and FORS2 on the VLT, and DEIMOS on Keck, to confirm both candidates beyond any doubt. We find redshifts of $z = 6.604$ and $z = 6.541$ for "CR7" and "MASOSA," respectively. "CR7" has an observed Lyα luminosity of $10^{43.93\pm0.05}$ erg s^{-1} (~3× more luminous than Himiko) and is the most luminous Lyα emitter ever found at the epoch of reionization.
2. MASOSA has a strong detection in Lyα, with very high Lyα EW (EW$_0$ > 200 Å), implying very low stellar mass and a likely extreme stellar population. It is, nonetheless, undetected in all other available bands and Lyα is also rather compact.
3. CR7, with a narrow Lyα line with 266 $\pm$ 15 km s^{-1} FWHM, is detected in the NIR (rest-frame UV), with $\beta = -2.3 \pm 0.08$, an excess in J band, and it is strongly detected in IRAC/*Spitzer*.
4. We detect a strong He II 1640 Å narrow emission line with both X-SHOOTER and SINFONI in CR7 (implying $z = 6.600$), which is enough to explain the clear excess seen in the J-band photometry. We find no other emission lines from the UV to the NIR in our X-SHOOTER spectra. No AGN line is seen, nor any signatures of WR stars, as the He II 1640 Å emission line is narrow (FWHM = 130 $\pm$ 30 km s^{-1}). The He II 1640 Å emission line implies that we are seeing the peak of Lyα emission redshifted by +160 km s^{-1} and thus that we are only seeing the red wing of the Lyα (the intrinsic Lyα flux is

thus likely much higher than seen), or we are witnessing an outflow.

5. The AGN and WR stars interpretation of the nature of CR7 are strongly disfavored. An alternative interpretation is that the source hosts a DCBH, although the lack of broad emission lines and the lack of X-ray detection also disfavors this interpretation. Given all the current data, we conclude that CR7 may host an unseen, extreme stellar population and it is therefore the strongest candidate for a PopIII-like stellar population found so far.
6. We find that CR7 cannot be described only by a PopIII stellar population, particularly due to the very strong IRAC detections. Our best interpretation of the full data (spectroscopy and photometry), which is fully consistent with many theoretical predictions, is a combination of a PopIII-like stellar population, which dominates the rest-frame UV and the emission lines, and an older, likely metal enriched stellar population, which is red, and that completely dominates the mass of the system. This interpretation fits remarkably well with high resolution *HST*/WFC3 imaging that reveals two red components, each about 5 kpc away from the peak of the rest-frame UV, Lyα and He II 1640 Å emission and that have the fluxes predicted by our SED fitting.

We may be witnessing, for the first time, direct evidence for the occurrence of waves of PopIII-like star formation which could happen from an original star cluster outward (resulting from strong feedback which can delay PopIII star formation), as suggested by, e.g., Tornatore et al. (2007). In this scenario, the reddest clump in CR7 (C, see Figures 7 and 8), which formed first (reddest and oldest), was likely responsible for not only starting to ionize a local bubble, but also for producing copious amounts of Lyman–Werner radiation and feedback that may have prevented star formation to occur in the vicinity of clump C. Star formation likely proceeded to the second clump once stellar feedback from C declined (B, see Figure 7), with similar effects (preventing star formation outside such a region, but further ionizing a local bubble), and we are observing source A (see Figure 7) at the right time to see an intense PopIII-like star formation episode. Most importantly, this scenario also provides a very simple explanation of why Lyα photons can easily escape the CR7 galaxy, as we see a significant amount of older stars that were able to emit a significant amount of UV photons for a few hundred million years before observations, enough to ionize a bubble of >1 Mpc around the source. Given the strong Lyman–Werner flux that we can infer is coming from the bright UV core, it is very likely that any previous episodes of star formation could have prevented the gas around those star-forming regions to form stars. Furthermore, we note that while radiation is able to affect the surroundings as it travels fast, significant metal enrichment is very inefficient on scales larger than ~1 kpc (e.g., Scannapieco et al. 2003; Tornatore et al. 2007; Ritter et al. 2014), both due to the larger timescales for metals (from supernovae) to travel outward (compared to the speed of light), but also due to the continued infall of metal-free gas from the cosmic web. It is therefore likely that in some cases, scales beyond 1–2 kpc of previous star formation activity can easily have the pristine gas necessary to allow PopIII to form (e.g., Ritter et al. 2012, 2014) even at $z \sim 6.6$, and to be detectable at redshifts even below $z \sim 5$ (e.g., Scannapieco et al. 2003; Tornatore et al. 2007). Tornatore et al. (2007), for example, predict that the peak of PopIII star formation rate density to occur at $z \sim 6$–8.

The spectroscopic confirmation of MASOSA and CR7, along with the high S/N spectroscopic and photometric data, allowed us to have a first glimpse into sources likely similar to Himiko and brighter, that are much more common than previously expected and have a remarkable nature. The follow-up of the full Matthee et al. (2015) Lyα sources at even higher luminosities found in the SA22 field will allow us to explore even more the diversity and nature of such unique targets. Such luminous Lyα emitters are the ideal first targets for *JWST*, particularly due to the likely very high EW and bright optical rest-frame emission lines, which may not be restricted to bright [O III] 5007, Hβ and Hα, but actually include He II 4686, He I4471, He I5016, and He I5876. In the case of CR7, a composite of a PopIII-like stellar population and a likely enriched stellar population which is physically separated by ~5 kpc (Figure 7) is currently strongly favored, and it is possible that similar stellar populations will be found in the other Lyα emitters. We may have found an actual population with clear signatures of PopIII-like stars, besides CR7. *JWST* will, in only a short exposure time, clearly show if the rest-frame spectra is made up of only He+H lines, confirming PopIII beyond any doubt, or if [O III] is also present and exactly where each of the lines is coming from.

We thank the anonymous reviewer for useful and constructive comments and suggestions which greatly improved the quality and clarity of our work. D.S. acknowledges financial support from the Netherlands Organisation for Scientific research (NWO) through a Veni fellowship, from FCT through a FCT Investigator Starting Grant and Start-up Grant (IF/01154/2012/CP0189/CT0010), from FCT grant UID/FIS/04434/2013, and from LSF and LKBF. J.M. acknowledges the award of a Huygens PhD fellowship. H.R. acknowledges support from the ERC Advanced Investigator program New-Clusters 321271. The authors thank Mark Dijkstra, Bhaskar Agarwal, Jarrett Johnson, Andrea Ferrara, Jarle Brinchmann, Rebecca Bowler, George Becker, Emma Curtis-Lake, Milos Milosavljevic, Raffaella Schneider, Paul Shapiro, and Erik Zackrisson for interesting, stimulating and helpful discussions. The authors are extremely grateful to ESO for the award of ESO DDT time (294.A-5018 and 294.A-5039) which allowed the spectroscopic confirmation of both sources and the detailed investigation of their nature. Observations are also based on data from W.M. Keck Observatory. The W.M. Keck Observatory is operated as a scientific partnership of Caltech, the University of California and the National Aeronautics and Space Administration. Based on observations obtained with MegaPrime/Megacam, a joint project of CFHT and CEA/IRFU, at the Canada–France–Hawaii Telescope (CFHT) which is operated by the National Research Council (NRC) of Canada, the Institut National des Science de lUnivers of the Centre National de la Recherche Scientifique (CNRS) of France, and the University of Hawaii. This work is based in part on data products produced at Terapix available at the Canadian Astronomy Data Centre as part of the Canada–France–Hawaii Telescope Legacy Survey, a collaborative project of NRC and CNRS. Based on data products from observations made with ESO Telescopes at the La Silla Paranal Observatory under ESO programme IDs 294.A-5018, 294.A-5039, and 179.A-2005, and on data products produced by

TERAPIX and the Cambridge Astronomy Survey Unit on behalf of the UltraVISTA consortium. The authors acknowledge the award of service time (SW2014b20) on the William Herschel Telescope (WHT). WHT and its service programme are operated on the island of La Palma by the Isaac Newton Group in the Spanish Observatorio del Roque de los Muchachos of the Instituto de Astrofisica de Canarias.

REFERENCES

Agarwal, B., Davis, A. J., Khochfar, S., Natarajan, P., & Dunlop, J. S. 2013, MNRAS, 432, 3438
Agarwal, B., Smith, B., Glover, S., et al. 2015, MNRAS, submitted (arXiv:1504.04042)
Appenzeller, I., Fricke, K., Fürtig, W., et al. 1998, Msngr, 94, 1
Atek, H., Kunth, D., Hayes, M., Östlin, G., & Mas-Hesse, J. M. 2008, A&A, 488, 491
Bacon, R., Brinchmann, J., Richard, J., et al. 2014, arXiv:1411.7667
Becker, R. H., Fan, X., White, R. L., et al. 2001, AJ, 122, 2850
Bolzonella, M., Miralles, J.-M., & Pelló, R. 2000, A&A, 363, 476
Bonnet, H., Abuter, R., Baker, A., et al. 2004, Msngr, 117, 17
Bouwens, R. J., Illingworth, G. D., Labbe, I., et al. 2011, Natur, 469, 504
Bouwens, R. J., Illingworth, G. D., Oesch, P. A., et al. 2015, ApJ, 803, 34
Bowler, R. A. A., Dunlop, J. S., McLure, R. J., et al. 2012, MNRAS, 426, 2772
Bowler, R. A. A., Dunlop, J. S., McLure, R. J., et al. 2014, MNRAS, 440, 2810
Brinchmann, J., Kunth, D., & Durret, F. 2008, A&A, 485, 657
Bromm, V., & Larson, R. B. 2004, ARAA, 42, 79
Bruzual, G., & Charlot, S. 2003, MNRAS, 344, 1000
Cai, Z., Fan, X., Jiang, L., et al. 2011, ApJL, 736, L28
Calzetti, D., Armus, L., Bohlin, R. C., et al. 2000, ApJ, 533, 682
Capak, P., Aussel, H., Ajiki, M., et al. 2007, ApJS, 172, 99
Caruana, J., Bunker, A. J., Wilkins, S. M., et al. 2014, MNRAS, 443, 2831
Cassata, P., Le Fèvre, O., Charlot, S., et al. 2013, A&A, 556, A68
Cassata, P., Tasca, L. A. M., Le Fèvre, O., et al. 2015, AAP, 573, A24
Cen, R., & Haiman, Z. 2000, ApJL, 542, L75
Ciardullo, R., Zeimann, G. R., Gronwall, C., et al. 2014, ApJ, 796, 64
Cooper, M. C., Newman, J. A., Davis, M., Finkbeiner, D. P., & Gerke, B. F. 2012, in Astrophysics Source Code Library, record ascl:1203.003
Cowie, L. L., & Hu, E. M. 1998, AJ, 115, 1319
De Breuck, C., Röttgering, H., Miley, G., van Breugel, W., & Best, P. 2000, A&A, 362, 519
Dijkstra, M. 2014, PASA, 31, 40
Dijkstra, M., Mesinger, A., & Wyithe, J. S. B. 2011, MNRAS, 414, 2139
Dijkstra, M., & Wyithe, J. S. B. 2007, MNRAS, 379, 1589
Eisenhauer, F., Abuter, R., Bickert, K., et al. 2003, Proc. SPIE, 379, 1548
Ellis, R. S., McLure, R. J., Dunlop, J. S., et al. 2013, ApJL, 763, L7
Elvis, M., Civano, F., Vignali, C., et al. 2009, ApJS, 184, 158
Erb, D. K., Pettini, M., Shapley, A. E., et al. 2010, ApJ, 719, 1168
Faisst, A. L., Capak, P., Carollo, C. M., Scarlata, C., & Scoville, N. 2014, ApJ, 788, 87
Fan, X., Strauss, M. A., Becker, R. H., et al. 2006, AJ, 132, 117
Faucher-Giguère, C.-A., Kereš, D., Dijkstra, M., Hernquist, L., & Zaldarriaga, M. 2010, ApJ, 725, 633
Finkelstein, S. L., Hill, G. J., Gebhardt, K., et al. 2011, ApJ, 729, 140
Finkelstein, S. L., Papovich, C., Dickinson, M., et al. 2013, Natur, 502, 524
Finlator, K., Davé, R., & Oppenheimer, B. D. 2007, MNRAS, 376, 1861
Furlanetto, S. R., Zaldarriaga, M., & Hernquist, L. 2004, ApJ, 613, 1
González, V., Bouwens, R., Illingworth, G., et al. 2014, ApJ, 781, 34
Gräfener, G., & Vink, J. S. 2015, arXiv:1505.02994
Greif, T. H., Springel, V., White, S. D. M., et al. 2011, ApJ, 737, 75
Guaita, L., Francke, H., Gawiser, E., et al. 2013, A&A, 551, A93
Hayes, M., Östlin, G., Schaerer, D., et al. 2010, Natur, 464, 562
Hirano, S., Hosokawa, T., Yoshida, N., et al. 2014, ApJ, 781, 60
Horne, K. 1986, PASP, 98, 609
Hu, E. M., Cowie, L. L., Barger, A. J., et al. 2010, ApJ, 725, 394
Ilbert, O., Capak, P., Salvato, M., et al. 2009, ApJ, 690, 1236
Iliev, I. T., Mellema, G., Pen, U.-L., et al. 2006, MNRAS, 369, 1625
Iye, M., Ota, K., Kashikawa, N., et al. 2006, Natur, 443, 186
Jimenez, R., & Haiman, Z. 2006, Natur, 440, 501
Johnson, J. L., Khochfar, S., Greif, T. H., & Durier, F. 2011, MNRAS, 410, 919
Karman, W., Caputi, K. I., Grillo, C., et al. 2015, A&A, 574, A11
Kashikawa, N., Nagao, T., Toshikawa, J., et al. 2012, ApJ, 761, 85
Kashikawa, N., Shimasaku, K., Matsuda, Y., et al. 2011, ApJ, 734, 119
Konno, A., Ouchi, M., Ono, Y., et al. 2014, ApJ, 797, 16
Lidman, C., Hayes, M., Jones, D. H., et al. 2012, MNRAS, 420, 1946
Madau, P. 1995, ApJ, 441, 18
Malhotra, S., & Rhoads, J. E. 2002, ApJL, 565, L71
Malhotra, S., & Rhoads, J. E. 2004, ApJL, 617, L5
Matsuda, Y., Yamada, T., Hayashino, T., et al. 2004, AJ, 128, 569
Matsuoka, K., Nagao, T., Maiolino, R., Marconi, A., & Taniguchi, Y. 2009, A&A, 503, 721
Matthee, J., Sobral, D., Santos, S., et al. 2015, arXiv:1502.07355
Matthee, J. J. A., Sobral, D., Swinbank, A. M., et al. 2014, MNRAS, 440, 2375
McCracken, H. J., Milvang-Jensen, B., Dunlop, J., et al. 2012, A&A, 544, A156
McQuinn, M., Zahn, O., Zaldarriaga, M., Hernquist, L., & Furlanetto, S. R. 2006, ApJ, 653, 815
Meiksin, A. 2005, MNRAS, 356, 596
Mesinger, A., Aykutalp, A., Vanzella, E., et al. 2015, MNRAS, 446, 566
Miyazaki, S., Komiyama, Y., Nakaya, H., et al. 2012, Proc. SPIE, 8446, 0
Miyazaki, S., Komiyama, Y., Sekiguchi, M., et al. 2002, PASJ, 54, 833
Mortlock, D. J., Warren, S. J., Venemans, B. P., et al. 2011, Natur, 474, 616
Murayama, T., Taniguchi, Y., Scoville, N. Z., et al. 2007, ApJS, 172, 523
Nagao, T., Sasaki, S. S., Maiolino, R., et al. 2008, ApJ, 680, 100
Nakajima, K., Ouchi, M., Shimasaku, K., et al. 2012, ApJ, 745, 12
Nakajima, K., Ouchi, M., Shimasaku, K., et al. 2013, ApJ, 769, 3
Newman, J. A., Cooper, M. C., Davis, M., et al. 2013, ApJS, 208, 5
Oesch, P. A., van Dokkum, P. G., Illingworth, G. D., et al. 2015, ApJL, 804, L30
Ono, Y., Ouchi, M., Mobasher, B., et al. 2012, ApJ, 744, 83
Ono, Y., Ouchi, M., Shimasaku, K., et al. 2010, ApJ, 724, 1524
Ouchi, M., Ellis, R., Ono, Y., et al. 2013, ApJ, 778, 102
Ouchi, M., Shimasaku, K., Akiyama, M., et al. 2008, ApJS, 176, 301
Ouchi, M., Shimasaku, K., Furusawa, H., et al. 2010, ApJ, 723, 869
Ouchi, M., Ono, Y., Egami, E., et al. 2009, ApJ, 696, 1164
Pentericci, L., Vanzella, E., Fontana, A., et al. 2014, ApJ, 793, 113
Prescott, M. K. M., Dey, A., & Jannuzi, B. T. 2009, ApJ, 702, 554
Raiter, A., Schaerer, D., & Fosbury, R. A. E. 2010, A&A, 523, A64
Ritter, J. S., Safranek-Shrader, C., Gnat, O., Milosavljević, M., & Bromm, V. 2012, ApJ, 761, 56
Ritter, J. S., Sluder, A., Safranek-Shrader, C., Milosavljevic, M., & Bromm, V. 2014, arXiv:1408.0319
Salpeter, E. E. 1955, ApJ, 121, 161
Scannapieco, E., Schneider, R., & Ferrara, A. 2003, ApJ, 589, 35
Schaerer, D. 2002, A&A, 382, 28
Schaerer, D. 2003, A&A, 397, 527
Schaerer, D., & de Barros, S. 2009, A&A, 502, 423
Schaerer, D., & de Barros, S. 2010, A&A, 515, A73
Schaerer, D., & Pelló, R. 2005, MNRAS, 362, 1054
Schaye, J., Crain, R. A., Bower, R. G., et al. 2015, MNRAS, 446, 521
Schenker, M. A., Ellis, R. S., Konidaris, N. P., & Stark, D. P. 2014, ApJ, 795, 20
Scoville, N., Abraham, R. G., Aussel, H., et al. 2007, ApJS, 172, 38
Shapiro, P. R., Giroux, M. L., & Babul, A. 1994, ApJ, 427, 25
Shibuya, T., Kashikawa, N., Ota, K., et al. 2012, ApJ, 752, 114
Shirazi, M., & Brinchmann, J. 2012, MNRAS, 421, 1043
Smit, R., Bouwens, R. J., Labbé, I., et al. 2014, ApJ, 784, 58
Sobral, D., Best, P. N., Geach, J. E., et al. 2009, MNRAS, 398, L68
Sokasian, A., Yoshida, N., Abel, T., Hernquist, L., & Springel, V. 2004, MNRAS, 350, 47
Stark, D. P., Richard, J., Siana, B., et al. 2014, MNRAS, 445, 3200
Steidel, C. C., Adelberger, K. L., Shapley, A. E., et al. 2000, ApJ, 532, 170
Steidel, C. C., Bogosavljević, M., Shapley, A. E., et al. 2011, ApJ, 736, 160
Steidel, C. C., Giavalisco, M., Pettini, M., Dickinson, M., & Adelberger, K. L. 1996, ApJL, 462, L17
Tilvi, V., Papovich, C., Finkelstein, S. L., et al. 2014, ApJ, 794, 5
Tornatore, L., Ferrara, A., & Schneider, R. 2007, MNRAS, 382, 945
Tumlinson, J., Giroux, M. L., & Shull, J. M. 2001, ApJL, 550, L1
Vanzella, E., Grazian, A., Hayes, M., et al. 2010, A&A, 513, A20
Verhamme, A., Schaerer, D., & Maselli, A. 2006, A&A, 460, 397
Vernet, J., Dekker, H., D'Odorico, S., et al. 2011, A&A, 536, A105
Vogelsberger, M., Genel, S., Springel, V., et al. 2014, MNRAS, 444, 1518
Westra, E., Jones, D. H., Lidman, C. E., et al. 2006, A&A, 455, 61
Yang, Y., Zabludoff, A. I., Davé, R., et al. 2006, ApJ, 640, 539
Zabl, J., Nørgaard-Nielsen, H. U., Fynbo, J. P. U., Laursen, P., Ouchi, M., & Kjærgaard, P. 2015, arXiv:1505.01859